Position and dynamics of the edge visible radiating belt at Wendelstein 7-X

T. Szepesi[1], C. Biedermann[2], B. Blackwell[3], S. Bozhenkov[2], G. Cseh[1], F. Effenberg[4], G. Fuchert[2], U. Hoefel[2], G. Kocsis[1], R. König[2], T. Sunn Pedersen[2], P. Drews[4], U. Wenzel[2], S. Zoletnik[1] and the W7-X Team

[1] *Wigner RCP RMI, Budapest, Hungary*

[2] *MPI für Plasmaphysik, Greifswald, Germany*

[3] *The Australian National University, Canberra, Australia*

[4] *University of Wisconsin, Madison, USA*

[5] *Forschungszentrum Juelich GmbH, Jülich, Germany*

A ten channel overview video diagnostic system was installed and commissioned at Wendelstein 7-X (W7-X) stellarator. In the first operation phase OP1.1, seven channels were equipped with EDICAMs, 1.3 Mpixel CMOS cameras (400 fps at full frame, up to 50 kfps at 64x64 pixel), observing the visible radiation emitted by the plasma [1]. In vast majority of the cases, visible radiation is found in a narrow layer/belt around the plasma edge, where the conditions are favourable for visible light emission. Since W7-X is a stellarator, the plasma is not toroidal-symmetric, and hence the observed edge radiation pattern (the image) detected by the tangentially viewing cameras does not resemble any of the toroidal cross-sections of a flux surface. Instead, the image intensity is highest in camera pixels where the line-of-sight corresponding to that particular pixel is tangent to the radiating belt.

A simple model was created to mimic the plasma radiation by assuming uniform and homogenous radiation all over a flux surface at a given effective minor radius r_{eff}. The width of the flux surface was assumed to be infinitesimally small, however, during the generation of a synthetic image the EDICAM camera sensor resolution was used, i.e. the minimum width of a structure was the pixel size. The synthetic image was generated by projecting toroidal cross-sections of the flux surface onto the camera sensor in 0.1° steps in the toroidal direction. The intensity of pixels was increased whenever one of these cross-sections touched the particular pixel. This way the synthetic images also predict which areas of the image can be expected to be the brightest. Comparison to real camera images shows good qualitative agreement (see Figure 1).

The synthetic images can be utilized to determine the plasma radius (r_{eff}) and the width of the visible radiating belt by convolving a camera image with a series of synthetic images generated for different r_{eff} values. For this investigation, masks are generated from the synthetic images so that pixels with brightness above a pre-defined threshold are set to 1,

while others are set to 0 values, in order to avoid false biasing of the "brightest" areas resulting from the assumption of homogeneous radiation distribution. Additionally, the result of the convolution (later on referred to as "mask radiation") is divided by the total of the "active" mask pixels (value = 1), i.e. the masks are normalized.

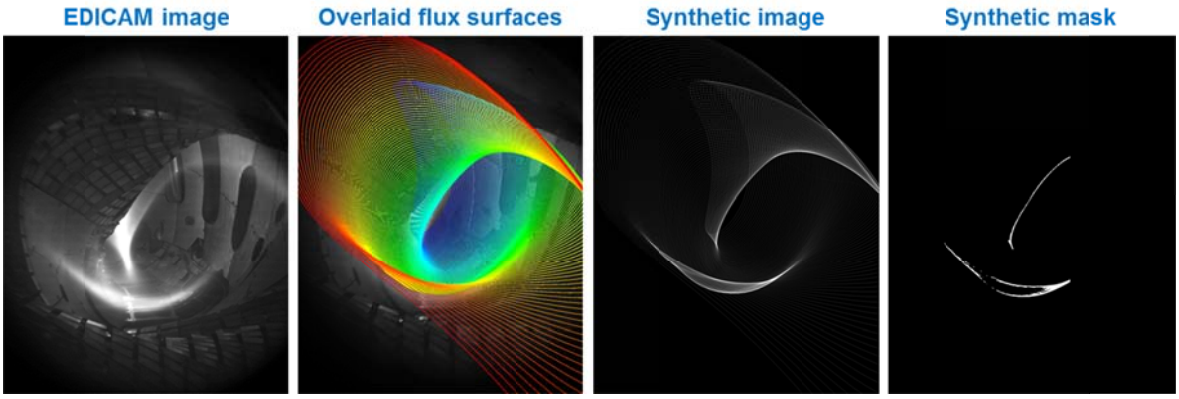

Figure 1. Modelling of the edge radiation seen by visible EDICAM cameras.

To test the applicability of this method, benchmark tests were carried out using synthetic images. Up to seven synthetic images corresponding to consecutive r_{eff} values (1-2 cm apart) were summed up to create a set of phantoms with different radiating belt width; these phantoms were used as inputs for the mask radiation method. In all cases, as expected, the mask radiation profile was found to be a single peak centered along the mean r_{eff}, with an FWHM proportional to the r_{eff} range of the source synthetic images. The relative error of the method was estimated to be 10%. The central r_{eff} value was successfully determined for each input phantom. Figure 2 (left) shows a case when only one synthetic image was used for the phantom. In this case, the radiating belt width is supposed to be zero, however, the resolution of the method is limited by the finite pixel size and the discrete number of r_{eff} values for which the synthetic images (and masks) were generated. The FWHM here thus corresponds to the technical resolution of the method, which can be regarded as an offset, and shall be further on subtracted from the result. This offset was found to be 21 mm. Figure 2 (right) shows the case when five synthetic images were used to create a phantom where the simulated radiating belt width was ca. 46 mm. For this case the FWHM was found to be 78 mm, yielding an estimated belt width of 57 mm with offset-correction, i.e. the relative error of the reconstruction is ca. 24%. Significantly better results can be obtained, however, when all seven phantoms are taken into account, and a linear fit is used to determine the offset (the y-intercept). It can be seen that the slope of the fit is close to 1, therefore the previous assumption of using a simple offset-correction to compensate for the finite resolution of the method is still valid. The offset value determined by the fit is 28 mm, yielding 50 mm for the 5-image-case in Figure 2, that is, the uncertainty could be reduced to ca. 10% – which coincides with the relative error of the data points.

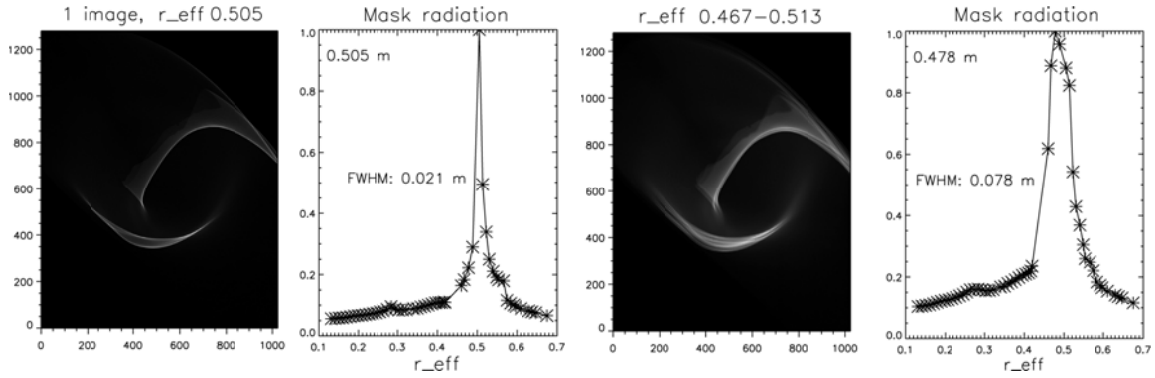

Figure 2. Phantoms generated using synthetic images. Left: a single image phantom close to the LCFS and the corresponding mask radiation profile. Right: a phantom composed of 5 synthetic images and the corresponding mask radiation profile.

As a next step, an EMC3-EIRENE simulation [2] was analysed with the mask radiation method. A phantom image was generated by projecting the 3D H-alpha radiation on the camera sensor plane. The location of the radiating belt was found to be at r_{eff} = 0.505 m, slightly outside the LCFS, with an FWHM of 113 mm, yielding a belt width of 85 mm (see Figure 3. right). Thus, according to this modelling, the radiating belt extends from the confined plasma edge to the near-SOL region.

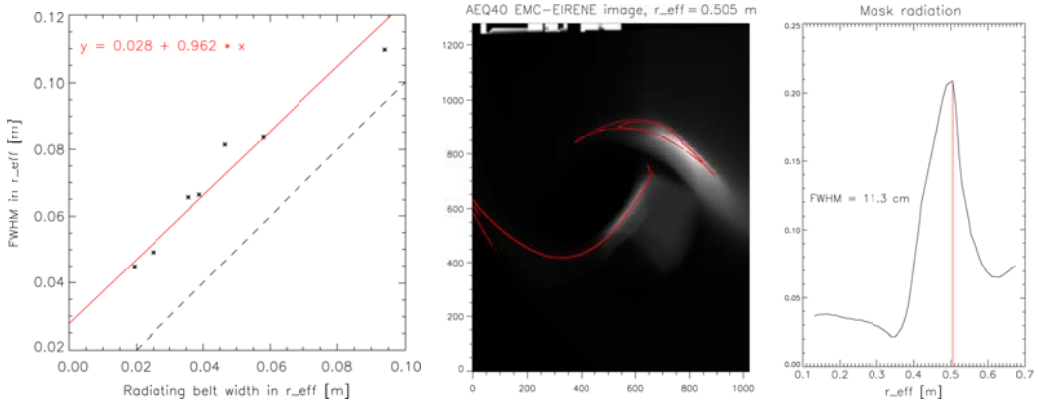

Figure 3. Left: Mask radiation FWHM vs the radiating belt width of phantoms. The dashed line is the y = x curve, in red a linear fit is plotted. Right: phantom of simulated H-alpha radiation and the corresponding mask radiation profile. Overplotted in red are the reconstructed r_{eff} and the corresponding synthetic mask.

The mask radiation method was applied to discharges where the midplane manipulator [3] was used. In a few discharges the maximum plunge depth was explored; in these experiments the manipulator head was closest to the LCFS in the whole OP1.1 campaign. One of these events is shown in Figure 4. On the left figure one can follow the evolution of the plasma size (denoted by the solid black line), from the build-up phase (first 50 ms) to the collapse (t = 0.6 – 0.72 s), while the right plot shows the width of the radiating belt. During the build-up and the collapse, the large values of the belt width result from the quickly evolving position of the belt, smeared by the relatively long exposure time (~10 ms) of the cameras.

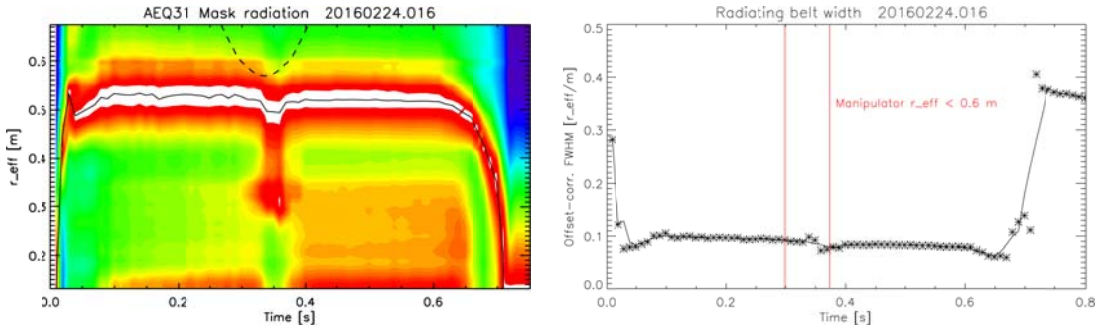

Figure 4. Left: Mask radiation (contour plot) with the reconstructed r_{eff} (solid black line) and the position of the midplane manipulator probe head (dashed line). Right: Radiating belt width for the same experiment.

It can be seen that when the manipulator approaches the plasma (closest point is 53 mm from the LCFS) radiation is significantly increased up to r_{eff} ~ 0.3 m, and the plasma minor radius shrinks ca. 4 cm to r_{eff} ~ 0.49 m. Additionally, the radiating belt width is slightly increased as a result of more intense release of impurities into the plasma from the manipulator head. When the manipulator quickly retracts, the belt width drops as the additional impurity source vanishes, and the original trend is restores within 2-30 ms as the plasma fills again the complete volume set by the limiters (at ca. t = 0.4 s).

The temperature of the radiating belt was found to be a few 10 eV in the plateau phase, based on limiter Langmuir probes [4]. When plasma collapse starts and the belt shrinks together with the plasma, the belt T_e decreases as well. Assumingly the n_e of the belt is increasing in a similar manner so that their product, proportional to the emitted light intensity, stays constant. However, density measurements are not validated yet to support this argument.

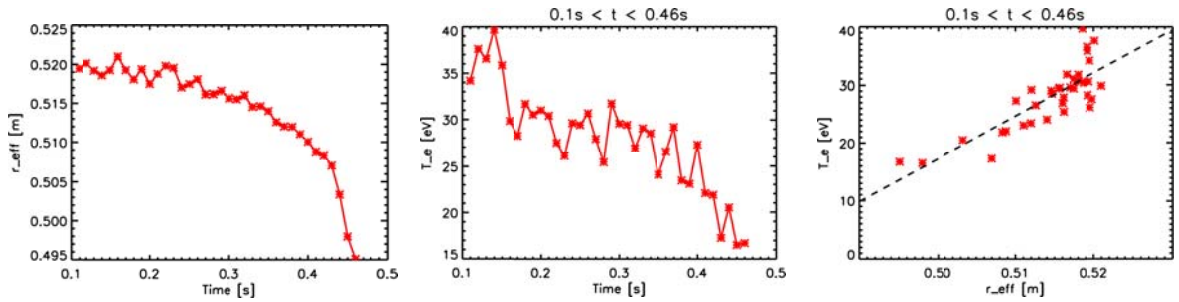

Figure 5. Effective radius (left) and T_e (mid) of the radiating belt vs time, T_e vs r_{eff} (right).

"This work has been carried out within the framework of the EUROfusion Consortium and has received funding from the Euratom research and training programme 2014-2018 under grant agreement No 633053. The views and opinions expressed herein do not necessarily reflect those of the European Commission."

[1] G. Kocsis et al, Fusion Engineering and Design **96-97** (2015) 808

[2] F. Effenberg et al, Nuclear Fusion **57** (2017) 036021

[3] D. Nicolai et al, doi.org/10.1016/j.fusengdes.2017.03.013

[4] M. Krychowiak et al, Review of Scientific Instruments **87** (2016) 11D304